Development of Braking Force Distribution Strategy for Dual-Motor-Drive Electric Vehicle

Binbin Sun*, Pengwei Wang, Song Gao, Jie Yu & Zhangu Wang

College of Transportation and Vehicle Engineering, Shandong University of Technology, 266# Xincun Road, Zibo City 255000, China
*E-mail: sunbin_sdut@126.com

Abstract. In the development of the optimal braking force distribution strategy for a dual-motor-drive electric vehicle (DMDEV) with a series cooperative braking system, three key factors were taken into consideration, i.e. the regenerative force distribution coefficient between the front and the rear motor (β), the energy recovery coefficient at the wheels (α_3), and the front-and-rear-axle braking force distribution coefficient (λ). First, the overall power loss model of the two surface-mounted permanent magnetic synchronous motors (SMPMSMs) was created based on the d-q axis equivalent circuit model. The optimal relationship of β and the overall efficiency of the dual-motor system were confirmed, where the latter was quite different from that obtained from the traditional look-up table method for the motors' efficiency. Then, four dimensionless evaluation coefficients were used to evaluate braking stability, regenerative energy transfer efficiency, and energy recovery at the wheels. Finally, based on several typical braking operations, the comprehensive effects of the four coefficients on braking stability and energy recovery were revealed. An optimal braking force distribution strategy balancing braking stability and energy recovery is suggested for a DMDEV with a series cooperative braking system.

Keywords: *braking stability; braking force distribution strategy; dual-motor-drive electric vehicle; energy recovery; overall power loss of dual-motor system.*

1 Introduction

Great efforts have been made to develop motor-drive train systems for electric vehicles to relieve the stresses caused by the fossil energy crisis and environmental pollution [1,2]. A distributed power train configuration with independently driving motors on the front and rear axle offers great flexibility and potential for optimization of vehicle performance [3,4]. Based on this configuration, several improvements have been achieved of vehicular driving characteristics, dynamic performance and failsafe control [5-8].

However, on braking force distribution, which has an important influence on vehicle braking performance and energy recovery [9,10], no systematic studies have been conducted yet. Generally speaking, researches have sufficiently

Received July 31st, 2017 Revised March 12th, 2018, Accepted for publication May 14th, 2018.
 ISSN: 2337-5779, DOI: 10.5614/j.eng.technol.sci.2018.50.2.3

considered vehicle safety, improvement of breaking reliability, breaking safety, and adaptability to different road conditions of breaking energy recovery systems [11] but ignored the perspective of energy recovery [12]. Optimal braking force distribution methods can satisfy both braking stability and energy recovery [13], while efficiency of breaking energy recovery can be improved greatly based on the safe principle [14], but it should be noted that the optimal distribution models based on the traditional look-up table method [15-18] actually ignore the effect of the non-work motor on braking performance, especially for permanent magnet synchronous motors (PMSM), as they still exhibit friction and iron losses [19,20]. Consequently, the look-up table method may lead to an incorrect torque distribution strategy, i.e. the partial-motor-operate mode takes precedence over the entire-motor strategy under low driving or severe braking conditions [21-23].

More importantly, for DMDEVs, apart from the optimal regenerative force distribution between the front and rear motors, two other factors are also crucial for developing a braking force distribution strategy. One is the braking force distribution coefficient between the front and rear axle related to braking stability [24,25], the other is the energy recovery of the wheels influencing energy recovery [26]. However, currently, the comprehensive effect of the three key factors on braking stability and energy recovery is still unconfirmed. Especially for DMDEVs with two SMPMSMs, there is no braking force distribution strategy that can balance braking stability and energy recovery.

This paper therefore presents a systemic study on the key factors of braking force distribution strategies for a DMDEV based on a series cooperative braking system [27] using new research methods. The proposed breaking force strategy confirms the key factors for breaking stability and energy recovery. The interaction mechanism of these key factors was explored and the influence of different braking feedback strategies on vehicle braking stability and energy recovery was quantitatively analyzed. First, the overall power loss model of the dual-motor system was established based on the mechanisms of the copper and iron loss in the SMPMSMs instead of the traditional look-up table method, and the optimal force distribution relationship between the front and rear regenerative system was derived; then, four dimensionless evaluation coefficients (C_λ, $C_{\alpha 3}$, C_β and *fit*) are proposed and their effect on braking stability and energy recovery are revealed; finally, an optimal regenerative braking force strategy, which balances breaking stability and energy recovery for the DMDEV with series cooperative braking system, is proposed.

2 Overview of DMDEV and Test Platform

2.1 Configuration of DMDEV

In the configuration of the DMDEV shown in Figure 1, the vehicle control unit (VCU) is the control center of the DMDEV. Based on the sampling signals, i.e. vehicle velocity (V) from the vehicle speed sensor, brake torque demand (T_{bd}) from the deceleration pedal (DP), and state of charge (SOC) from the battery management system (BMS), the VCU generates control commands for the rear motor control unit (MCU1), the front motor control unit (MCU2), and the hydraulic brake controller (HBC) to achieve braking torque control. Moreover, for the DMDEV proposed in this study, two one-speed gearboxes are equipped to achieve torque transmission. The total reduction ratios of the front and rear transmission system are both 5:1.

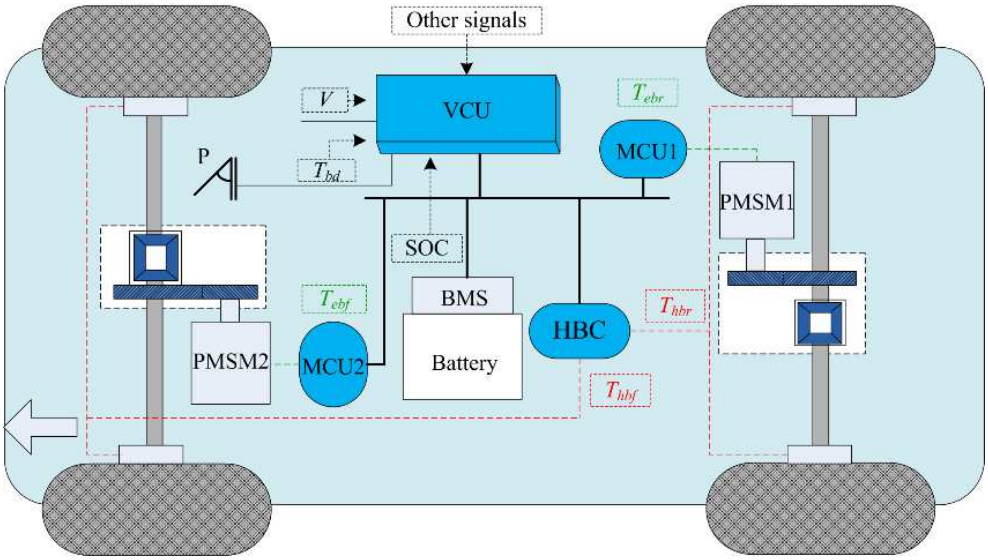

Figure 1 Configuration of the DMDEV.

3 Effect of β on Overall Efficiency of Dual-Motor System

3.1 Braking Energy Flow of DMDEV

During the braking process of the DMDEV, only a small proportion of the vehicular kinetic energy is utilized to overcome the air and rolling resistance, while most of it is translated into thermal and electric energy through the cooperative braking system. For the braking energy flow of the DMDEV shown in Figure 2, reducing the energy loss in the energy transfer process from wheels

to battery is the key to improving energy recovery efficiency, which consists of efficiency optimization of the front and rear transmission systems (η_{Tf} and η_{Tr}) and the dual-motor system (η_{mf} and η_{mr}).

As the front and rear transmission and differential systems (FTD and RTD) in the DMDEV are identical, η_{Tf} can be taken as equal to η_{Tr}; both are equivalent to a constant in this study. The energy recovered into the battery can be expressed as follows:

$$E_{re} = \alpha_3 \eta_{Tf} \eta_b \left[\beta \eta_{mf} + (1-\beta) \eta_{mr} \right] E_t \tag{1}$$

where α_3 is the proportion of the vehicular kinetic energy recovered at the wheels, η_b is the charging efficiency of the battery system, E_t is the kinetic energy of the dual-motor-drive electric vehicle, β is the regenerative energy distribution coefficient, which is the ratio between the regenerative energy distributed to the front wheels and the total regenerative energy. Under a given braking operation, β can be expressed as follows:

$$\beta = \frac{\sum_{i=1}^{k} \frac{T_{ebf\_i}}{r} V_i \frac{t_1 - t_0}{k}}{\sum_{i=1}^{k} \frac{T_{ebf\_i}}{r} V_i \frac{t_1 - t_0}{k} + \sum_{i=1}^{k} \frac{T_{ebr\_i}}{r} V_i \frac{t_1 - t_0}{k}} \tag{2}$$

where T_{ebf} and T_{ebr} are the regenerative braking torques at front and rear wheel, t_0 and t_1 are the times when the braking operation happens and finishes, r represents the wheel radius, V_i is the vehicle velocity at sampling point i, k is the number of sampling points during the braking process. Moreover, if k is large enough, β can be simplified as shown in Eq. (3), which means that β can also be regarded as the ratio between the regenerative braking torque at the front wheels and the total regenerative braking torque.

$$\beta = \frac{\sum_{i=1}^{k} T_{ebf\_i}}{\sum_{i=1}^{k} T_{ebf\_i} + \sum_{i=1}^{k} T_{ebr\_i}} \tag{3}$$

Based on the above analysis, different β values mean variation of T_{ebf} and T_{ebr} under a given braking operation, which thus affects η_{mf} and η_{mr}. Therefore, Eq. (1) can be simplified as follows:

$$E_{re} = \alpha_3 \eta_{Tf} \eta_b G(\beta) E_t \tag{4}$$

where $G(\beta)$ is the overall efficiency of the dual-motor system, which can be expressed as follows:

$$G(\beta) = \beta f_1(\beta) + (1-\beta) f_2(\beta) = \frac{P_{sys\_out}}{P_{sys\_out} + P_{tl\_loss}} \tag{5}$$

where P_{sys_out} is the output power of the dual-motor system, P_{tl_loss} represents the overall power loss of the dual-motor system, which has a direct influence on $G(\beta)$. Therefore, how to minimize P_{tl_loss} is the key to improving $G(\beta)$ under given braking operations.

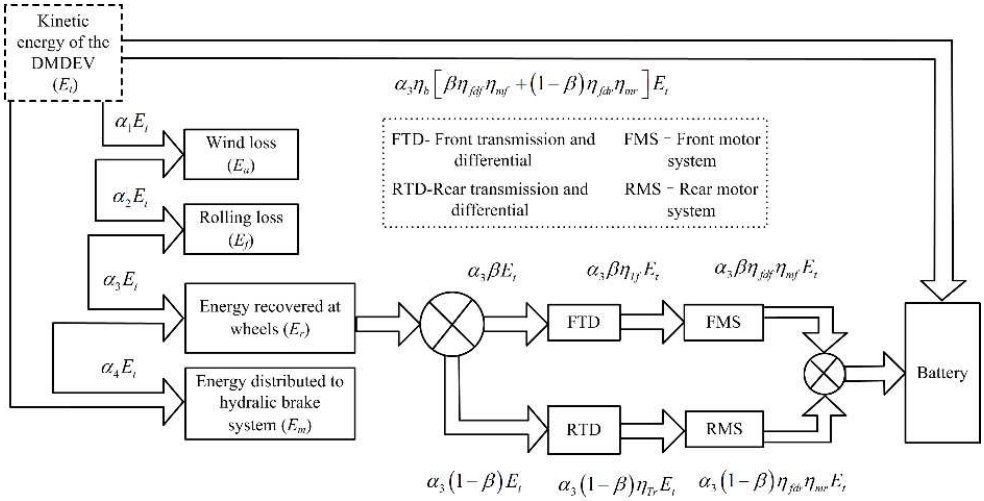

Figure 2 Braking energy flow of the DMDEV.

3.2 Derivation of Dual-motor Power Loss

The power loss of a PMSM consists of friction loss (P_m), which is mainly proportional to motor speed; stray loss (P_s), which is relatively small; copper loss (P_{cu}), which is produced by the electrical current in the stator; and iron loss (P_{iron}), which consists of hysteresis and eddy current loss as a result of the changing magnetization in the motor.

Of the four categories of power loss in a PMSM, P_{cu} and P_{iron} are closely related to the current in the motor stator. Furthermore, as field-oriented control is used for the two SMPMSMs in this study, variation of β will have an impact on P_{cu} and P_{iron} as a result of the changing T_{ebf} and T_{ebr}. In other words, $G(\beta)$ is a function of the copper and iron loss (See Eq. (6)):

$$G(\beta) = f\left(P_{cu\_tl}, P_{iron\_tl}\right) \tag{6}$$

where P_{cu_tl} is the overall copper loss of the SMPMSMs, P_{iron_tl} is the total iron loss of the motors.

To establish the power loss model of the PMSM, *d-q* axis equivalent circuit mode was adopted [28,29]. Based on the equivalent circuit model, the copper loss and the iron loss in the PMSM can be expressed in Eq. (7) as follows:

$$\begin{aligned} P_{cu} &= R_s\left[\left(i_{dc}+i_{dt}\right)^2+\left(i_{qc}+i_{qt}\right)^2\right] \\ P_{iron} &= R_c\left({i_{dc}}^2+{i_{qc}}^2\right) \end{aligned} \tag{7}$$

where i_{dc} and i_{dt} are the *d*-axis stator currents divided into iron loss current and torque current, i_{qc} and i_{qt} represent the iron loss current and the torque current from the *q*-axis stator current. R_s is the armature resistance of the stator, and R_c is the equivalent resistance of the iron loss.

1) First, when the SMPMSM operates in the base speed area, to achieve the maximum torque per ampere control, i_d is set to 0. Given the above analysis, P_{cu} and P_{iron} are obtained in Eqs. (8) & (9) as follows:

$$P_{cu} = R_s\left[\left(\left(\frac{Vf_dL_m}{rR_c}\right)^2+1\right)\frac{T_{eb}}{P\psi_f}+\frac{Vf_d\psi_f}{rR_c}\right]^2 \tag{8}$$

$$P_{iron} = \left(\frac{V^2{f_d}^2}{r^2R_c}\right)\left[\left(\frac{Vf_d{L_m}^2}{rR_c}\frac{T_{eb}}{P\psi_f}+\psi_f\right)^2+\left(\frac{L_mT_{eb}}{P\psi_f}\right)^2\right] \tag{9}$$

where f_d is the total gear ratio of the FTD or the RTD system, r is the wheel radius, T_{eb} is the electromagnetic torque, P is the number of pole pairs, L_m is the mutual inductance, ψ_f is flux linkage.

To simplify the derivation process, set $\left(\frac{Vf_dL_m}{rR_c}\right)^2+1=a$, $P\psi_f=b$, $\frac{Vf_d\psi_f}{rR_c}=c$, $\frac{V^2{f_d}^2}{r^2R_c}=d$ and $\frac{Vf_d{L_m}^2}{rR_c}=k$. The total copper loss of the dual-motor system can be obtained in Eq. (10) as follows:

$$P_{cu\_tl} = R_{sf}\left[\frac{a_f\beta T_{eb}}{b_f}+c_f\right]^2+R_{sr}\left[\frac{a_r\left(1-\beta\right)T_{eb}}{b_r}+c_r\right]^2 \tag{10}$$

where the subscripts *f* and *r* mean the front and rear SMPMSM, respectively.

The performance parameters of the front and rear power train system are the same as those mentioned above in Section 2, $P_f = P_r$, $\psi_{ff} = \psi_{fr}$ and $f_{df} = f_{dr}$. Moreover, since it is the motor speed rather than the motor torque that has a significant effect on R_c[27], as shown in Figure 3, R_{cf} can be considered equal to R_{cr} under a given braking severity. In summary, the overall copper loss of the two motors under a given braking operation can be simplified in Eq. (11) as follows:

$$P_{cu\_tl} = R_s\left[\frac{a\beta T_{eb}}{b} + c\right]^2 + R_s\left[\frac{a(1-\beta)T_{eb}}{b} + c\right]^2 \tag{11}$$

Using the same methods, the total iron loss of the two motors under a given braking operation can be derived from Eq. (12) as follows:

$$\begin{aligned} P_{iron\_tl} = {} & d\left[\left(k\frac{\beta T_{eb}}{b} + \psi_f\right)^2 + \left(\frac{L_m \beta T_{eb}}{b}\right)^2\right] + \\ & d\left[\left(k\frac{(1-\beta)T_{eb}}{b} + \psi_f\right)^2 + \left(\frac{L_m(1-\beta)T_{eb}}{b}\right)^2\right] \end{aligned} \tag{12}$$

Based on the above analysis, under a given braking operation, the overall power loss of the two SMPMSMs in the base speed area is confirmed in Eq. (13) as follows:

$$P_{tl} = P_{cu\_tl} + P_{iron\_tl} + P_{mf} + P_{mr} + P_{sf} + P_{sr} \tag{13}$$

where P_{mf} and P_{mr} are the friction losses of the front and rear SMPMSM, which are mainly influenced by the motor speed instead of the motor torque [30]. Under any given condition, a change in β has little influence on both. Consequently, the friction loss is ignored during the derivation of the optimal β. P_{sf} and P_{sr} are the stray losses of the front and rear motor. As they are not only quite small compared with other losses in the SMPMSM but also difficult to calculate accurately [31], they are not dealt with in the dual-motor-loss model.

2) Secondly, when the SMPMSM operates in the flux-weakening domain, to achieve flux-weakening control, i_d is expressed in Eq. (14) as follow:

$$i_d = \frac{-\psi_f}{L_m} + \sqrt{\left(\frac{U_{\max}}{\omega L_m}\right)^2 - i_q^{\,2}} \tag{14}$$

where U_{max} is the maximum phase voltage.

Referring to the modeling method of P_{cu_tl} and P_{iron_tl} in the base speed area, the total copper and iron loss of the two motors in flux-weakening domain can be obtained in Eqs. (15) & (16) as follows:

$$P_{cu\_tl} = R_s 2\left(\frac{\psi_f}{L_m}\right)^2 + 2g^2 R_s - \frac{2\psi_f R_s}{L_m}\left(\sqrt{g^2 - \left(\frac{\beta T_{eb}}{b}\right)^2} + \sqrt{g^2 - \left(\frac{(1-\beta)T_{eb}}{b}\right)^2}\right) \tag{15}$$

$$P_{iron\_tl} = \frac{rL_m {T_{eb}}^2}{Vf_d R_c b}\left(2\beta^2 - 2\beta + 1\right) + 2{T_{eb}}^2\sqrt{(\beta g)^2 - \left(\frac{\beta^2 T_{eb}}{b}\right)^2} + 2{T_{eb}}^2\sqrt{\left((1-\beta)g\right)^2 - \left(\frac{(1-\beta)^2 T_{eb}}{P\psi_f}\right)^2} \tag{16}$$

where $g = \dfrac{U_{max} r}{L_m V f_d}$.

3.3 Optimal β Aimed at Least Overall Power Loss

In the base speed area of the SMPMSM, under a given braking operation, to find the optimal β aimed at the least overall power loss, the first- and second-order partial derivatives of β in Eq. (14) are obtained as shown in Eqs. (17) and (18):

$$\frac{\partial P_{tl}}{\partial \beta} = \left[2R_s\left(\frac{aT_{eb}}{b}\right)^2 + 2d\left(\frac{T_{eb}}{b}\right)^2\left(k^2 + {L_m}^2\right)\right](2\beta - 1) \tag{17}$$

$$\frac{\partial^2 P_{tl}}{\partial \beta^2} = 2\left[2R_s\left(\frac{aT_{eb}}{b}\right)^2 + 2d\left(\frac{T_{eb}}{b}\right)^2\left(k^2 + {L_m}^2\right)\right] > 0 \tag{18}$$

Based on the first-order partial derivative of β shown in Eq. (18), an extreme value of P_{tl} can be obtained when β is 0.5. Furthermore, the characteristic of the second-order partial derivative ($\dfrac{\partial^2 P_{tl}}{\partial \beta^2} > 0$) reveals that the relationship of P_{tl} and β is concave nearby β = 0.5, which indicates that the minimum P_{tl} can be obtained if β is set to 0.5. In other words, the dual-motor system is capable of

achieving the maximum overall efficiency when β is 0.5 during the regenerative braking process.

4 Multi-Factor Evaluation Model for Braking Force Distribution Strategy of DMDEV

Apart from the optimal β derived above, λ (the braking force distribution coefficient between front and rear axle) and α_3, which affect braking stability and braking economy respectively, are also crucial for developing a multi-objective braking force distribution strategy.

4.1 Constraints of Braking Stability

As for braking stability, the ideal relationship between the front and rear braking force at the wheels can be expressed in Eq. (19) as follows:

$$\begin{aligned} F_{\mu r} &= \frac{1}{2}\left[\frac{G}{h_g}\sqrt{L_r^{\,2}+\frac{4h_g L}{G}F_{\mu f}}-\left(\frac{GL_r}{h_g}+2F_{\mu f}\right)\right] \\ \lambda_I &= \frac{F_{\mu f}}{F_{\mu r}} = \frac{L_r+\varphi h_g}{L_f-\varphi h_g} \end{aligned} \tag{19}$$

As shown in Figure 3, h_g is the height of the vehicular mass center, L_f and L_r represent the lengths between the automotive centroid and the center line of the front and rear axle, respectively, F_{uf} and F_{ur} are the braking forces at the front and the rear wheels, while G is the no-load weight of the DMDEV.

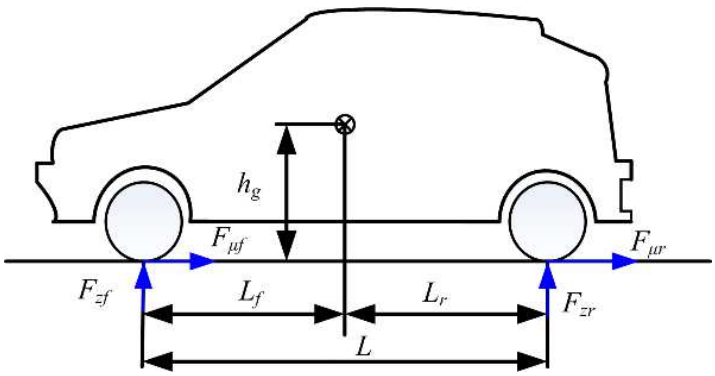

Figure 3 Forces acting on DMDEV braking on a level road.

Moreover, in order to avoid rear wheel lock preceding front wheel during the braking process, which may result in instability of the vehicle, the braking forces at the front and the rear wheels have to meet ECE regulations [32].

Specifically, for a roadway with road adhesion coefficient between 0.2 and 0.8, the constrained boundaries of the braking forces at the front and the rear wheels are expressed in the following Eq. (20):

$$\begin{cases} F_{\mu f} = \dfrac{Z+0.07}{0.85}\dfrac{G}{L}\left(L_r + Zh_g\right) & 0.2 \le Z \le 0.8 \\ F_{\mu r} = GZ - F_{\mu f} \end{cases} \tag{20}$$

In addition, when the breaking severity (Z) changes within the range between 0.3 and 0.5, the braking forces at the front and rear wheels also need to meet the other boundary conditions, as shown in the following Eq. (21):

$$\begin{aligned} F_{\mu r} &= \left(Z+0.05\right)\frac{G}{L}\left(L_f - Zh_g\right) \\ F_{\mu f} &= GZ - F_{\mu r} \end{aligned} \tag{21}$$

4.2 Evaluation Parameters for Braking Stability and Energy Recovery

To establish a multi-factor evaluation model for the braking force distribution strategy of a DMDEV, in this study, four dimensionless evaluation coefficients (C_λ, C_β , $C_{\alpha 3}$ and *fit*) are proposed.

Firstly, C_λ is the relationship between the ideal λ_I and the actual λ_a as shown in Eq. (22), which is used to evaluate the braking stability. Better braking stability can be achieved if C_λ is closer to 1 under a given braking severity.

$$\begin{aligned} C_\lambda &= \frac{\lambda_I}{\lambda_a} \quad \text{if} : \lambda_a < \lambda_I \\ C_\lambda &= \frac{\lambda_a}{\lambda_I} \quad \text{if} : \lambda_a < \lambda_I \end{aligned} \tag{22}$$

In addition, as shown in Eq. (23), the effect of the non-work SMPMSM on λ_a is taken into consideration in this study, where friction and iron losses still exist and both of them actually act as mechanical braking force (F_{dmr}), as shown in Figure 3.

$$\begin{aligned} \lambda_a &= \frac{F_{ebf} + F_{mbf}}{F_{ebr} + F_{mbf} + sign\left(\beta\right)\overline{F}_{dmr}} \\ &\begin{cases} sign\left(\beta\right) = 0 & \text{if} : 0 < \beta < 1 \\ sign\left(\beta\right) = 1 & \text{if} : \beta = 1 \end{cases} \end{aligned} \tag{23}$$

where $\overline{F}_{dmr}$ is the average value of F_{dmr}, which is the function of motor speed during the braking process, as shown in Figure 3; F_{eb} and F_{mb} are the regenerative and mechanical braking forces; while the subscripts f and r represent the front and rear motor.

Secondly, C_β is proposed to evaluate the transfer efficiency of the dual-motor system, which is the ratio between the actual overall efficiency of the dual-motor system and the optimal overall efficiency under a given braking intensity (See Eq. (24)).

$$C_\beta = \frac{\overline{G(\beta)}_{\_T_{ebact}}}{\overline{G(0.5)}_{\_T_{ebmax}}} \tag{24}$$

where the subscript T_{ebact} is the actual output torque of the dual-motor system; T_{ebmax} is the maximum regenerative torque that can be provided by the dual-motor system under a given braking severity; $\overline{G(\beta)}$ is the mean value of the overall efficiency, which is a function of motor speed.

Furthermore, to evaluate the energy recovered at the front and the rear wheels, as shown in Figure 2, which has an impact on the total energy recovery, $C_{\alpha 3}$ is proposed as in the following Eq. (25):

$$C_{\alpha 3} = \frac{\int_{t0}^{t1} F_{eb} V dt}{\int_{t0}^{t1} \left(F_{eb} + F_{mb} + F_f + F_a + sign(\beta)\overline{F}_{dmr}\right) V dt dt}$$
$$\begin{cases} sign(\beta) = 0 & \text{if}: 0 < \beta < 1 \\ sign(\beta) = 1 & \text{if}: \beta = 1 \end{cases} \tag{25}$$

where F_f and F_a are the resistances caused by tire rolling and wind drag, which are relatively small compared to the braking force. Under a given brake pedal degree, both F_{eb} and F_{mb} can be viewed as stationary during the braking process. In summary, the factor of $C_{\alpha 3}$ can be simplified in EQ. (26) as follows:

$$C_{\alpha 3} = \frac{F_{eb}}{F_{eb} + F_{mb} + sign(\beta)\overline{F}_{dmr}}$$
$$\begin{cases} sign(\beta) = 0 & \text{if}: 0 < \beta < 1 \\ sign(\beta) = 1 & \text{if}: \beta = 1 \end{cases} \tag{26}$$

Finally, given the above analysis, a multi-factor evaluation model (fit) for the braking force distribution strategy of the DMDEV is proposed in Eq. (27) as follows:

$$fit(i) = W_1 C_\lambda + W_2 C_\beta + W_3 C_{\alpha 3} \tag{27}$$

where W_1, W_2 and W_3 are weight coefficients, and i represents the braking strategy point.

5 Effect of Multiple Factors on the Braking Performance of the DMDEV

5.1 Design of Experiments

As shown in Figure 1, V, T_{bd} (Z) and SOC, which characterize the braking operation, are the reference signals for the regenerative braking control. Since it is unpractical to analyze the effect of multiple factors on braking performance for every possible braking operation based on a test method, four typical braking severities were chosen (Z = 0.1, Z = 0.23, Z = 0.4 and Z = 0.65) to study the deceleration processes of the DMDEV, as shown in Figure 4.

Designs for three levels of factor V (20 km/h, 40 km/h and V = 60 km/h) were adopted to characterize urban driving conditions, where a reasonable regenerative braking force distribution strategy plays an important role in the improvement of vehicle economy.

Table 1 Design of braking operations.

V	Z			
/km.h^{-1}	**0.1**	**0.23**	**0.4**	**0.65**
20	Case 1	Case 2	Case 3	Case 4
40	Case 5	Case 6	Case 7	Case 8
60	Case 9	Case 10	Case 11	Case 12

In addition, as the SOC signal is mainly utilized to restrict regenerative braking force under high levels (SOC > 85%, generally), a single-level SOC (SOC = 40%) was designed. Given the above analysis, under the level of SOC = 40%, a test graph with 2 multilevel factors (3 levels for V and 4 levels for Z) was designed, as shown in Table 1. For each case in Table 1, test points (colored blue in Figure 4) were designed to study the effect of the various braking force distribution strategies on energy recovery and braking stability. A_{2_1} and A_{2_2} are the supplements for A_2; their coordinates represent the regenerative forces.

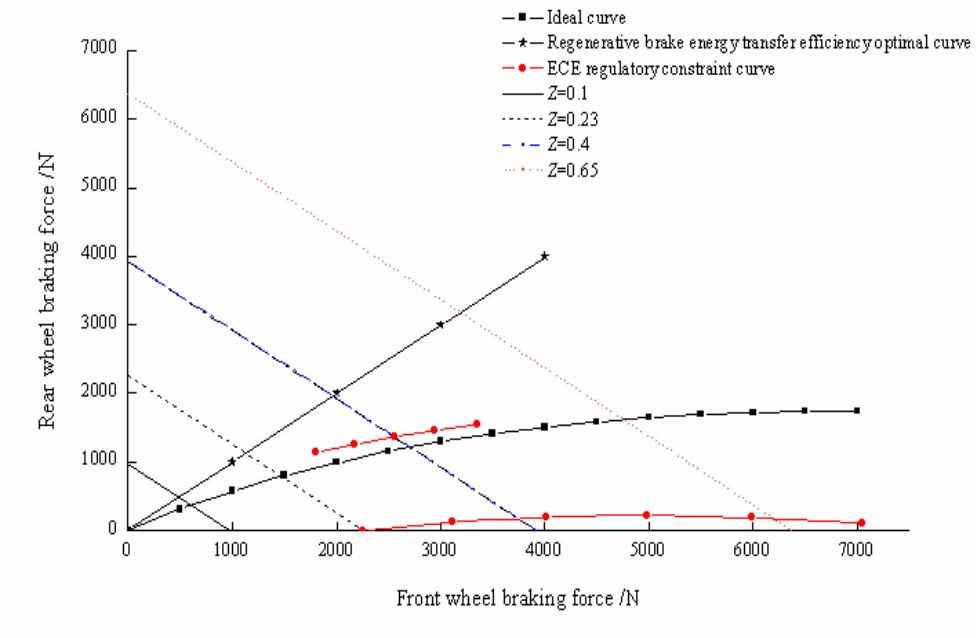

Figure 4 Test points for each designed case.

5.2 Discussions of Test Results

5.2.1 Case 5

When ignoring the effect of β on dual-motor transfer efficiency, strategy point A_3 in Figure 4 is the preferred braking force distribution for energy recovery based on the traditional look-up-table method. However, actually, as shown in Table 2, in comparison with other points on line A_1-A_3, when considering factor C_β, the worst energy recovery and comprehensive index are obtained at point A_3, which indicates that the effect of the non-work SMPMSM needs to be taken into account when designing a braking force distribution strategy for the dual- or multi-motor drive train EV.

Table 2 Results of regenerative braking performance for case 5.

Strategy points	Evaluation parameters			
	C_β	C_{a3}	C_λ	*fit*
A_1	0.9964	1	1	2.9964
A_2	0.9679	1	0.4203	2.3882
A_{2_1}	0.9720	0.4	0.4203	1.7923
A_{2_2}	0.9657	0.8889	0.4203	2.2749
A_3	0.9107	0.9521	0.0982	1.961
$A_{3\text{-}1}$	0.9107	0.9521	0.0982	1.961

Table 3 Results of regenerative braking performance for case 6.

Strategy points	Evaluation parameters			
	C_β	$C_{\alpha 3}$	C_λ	C_f
E_1	0.9923	1	1	2.9923
E_2	0.9962	0.8518	0.4680	2.3138
E_{3_1}	0.9232	0.6353	0.0486	1.5943

Table 4 Results of regenerative braking performance for case 7.

Strategy points	Evaluation parameters			
	C_β	$C_{\alpha 3}$	C_λ	C_f
X_1	0.9992	0.7236	0.8362	2.559
X_2	0.9980	0.6848	1	2.6828
X_3	0.9292	0.3750	0.1402	1.4444

Table 5 Results of regenerative braking performance for case 8.

Strategy points	Evaluation parameters			
	C_β	$C_{\alpha 3}$	C_λ	C_f
Y_1	0.9992	0.41	1	2.4092
Y_2	0.9932	0.3594	0.5278	1.8804
Y_3	0.9266	0.2309	0.0078	1.1653

Moreover, as shown in Table 2, for braking operations with low brake strength, the optimal distribution strategy that can balance braking stability and energy recovery is strategy point A_1, where the optimal C_f is obtained. In addition, at strategy points A_2, A_{2_2} and A_{2_1}, $C_{\alpha 3}$ gets smaller due to the increase in the proportion of mechanical braking force. Furthermore, at strategy point A_{2_1}, although β is 0.5 (T_{ed} = -18 N.m, T_{ebf} = T_{ebr} = -9 N.m), C_β is still worse than point A_1 (β = 0.6238, T_{ed} = -45 N.m) due to the smaller overall efficiency of the dual-motor system when regenerative braking torque is small.

5.2.2 Case 6

For braking in this case, at distribution point E_3, the front regenerative braking system outputs the maximum allowed braking force. Based on the test results shown in Table 3, strategy point E_1 is the optimal distribution strategy for this braking condition, where the optimal C_f is obtained, and both braking stability and energy recovery can be satisfied. Moreover, due to the increase in the proportion of mechanical braking force, $C\alpha_3$ gets smaller from points E_1 to E_3.

5.2.3 Case 7

In this case, as shown in Table 4, since better $C\alpha_3$ can be achieved owing to the larger regenerative braking force provided by the rear regenerative braking system, strategy point X_1 is superior to X_2 from the perspective of energy

recovery. However, another thing should be noted: distribution point X_2 is still preferred to X_1 because of the optimal multi-factor evaluation index for this strategy point, which indicates that strategy point X_2 can better meet both braking stability and energy recovery.

5.2.4 Case 8

As shown in Table 5, the braking characteristics of the designed strategy points in Case 8 are similar to the results of Case 6. First of all, for distribution points Y_1, Y_2 and Y_3, the braking energy that is distributed to the regenerative braking system ($C\alpha_3$) decreases as a result of the increase of the mechanical braking force. Secondly, the optimal C_f is obtained at strategy point Y_1. In addition, for braking cases with relatively high braking strengths, mainly due to the significant reduction of $C\alpha_3$, the braking energy that can be recovered into the battery system is quite small.

5.2.5 Cases 5 and 6

By comparing strategy point A_1 with E_1, it can be confirmed that, with the enlargement of Z, the losses caused by wind drag and rolling resistance decrease and thus the proportion of the vehicle kinetic energy recovered at the wheels (α_3) increases, as shown in Table 6. On the other hand, as shown in Table 2 and 3, the difference of energy recovered into the battery at strategy point A_1 and E_1 is relatively small as a result of the deterioration of the dual-motor operating efficiency ($\overline{G(\beta)}$) and the battery charging efficiency ($\overline{\eta_b}$), as shown in Table 5. Comparison between A_1 and E_1 indicates that β is a key factor that influences energy recovery under low braking strengths.

Table 6 Results of regenerative braking performance.

Strategy points	Performance parameters		
	α_3	$\overline{G(\beta)}$	$\overline{\eta_b}$
A_1	0.8023	0.8200	0.7926
E_1	0.9142	0.7634	0.7575
X_2	0.5794	0.7746	0.6699
Y_1	0.3060	0.7725	0.6084

5.2.6 Cases 6, 7 and 8

With the increase of braking severity (from 0.205 to 0.65), taking the distribution points E_1, X_2, and Y_1, for example, limited by the maximum allowed regenerative force, greater mechanical braking force is required to meet vehicle braking severity. Consequently, braking energy that is distributed to a

regenerative system reduces significantly. As shown in Table 6, the α_3 at strategy points X_2 and Y_1 are reduced by 39.95% and 60.61% compared with the one at point E_1, which reveals that α_3 is a key factor that influences energy recovery with the increase of braking severity.

5.2.7 All Cases Studied in this Paper

Figure 5 presents the multi-factor fitness values for the designed braking operations. Generally, for a given braking severity, the velocity factor has little influence on the multi-factor fitness value (C_f). More importantly, for the DMDEV with series cooperative braking system studied in this paper, both braking stability and energy recovery can be achieved if the braking force distribution strategy follows the rules described below:

1. Firstly, from the perspective of λ, braking force distribution between the front and rear axle should adhere to the ideal curve of λ_I shown in Figure 4.
2. Based on the constraint proposed above, at the second level of β and α_3, firstly, regenerative braking force is preferred; secondly, the hydraulic braking system participates in cooperative braking only when the regenerative braking force is insufficient to meet the given braking severity.
3. However, for the cases with high braking intensities ($Z > 0.7$), when the braking energy that can be recovered into the battery is quite small, only the hydraulic braking system participates in vehicle braking to ensure braking safety.

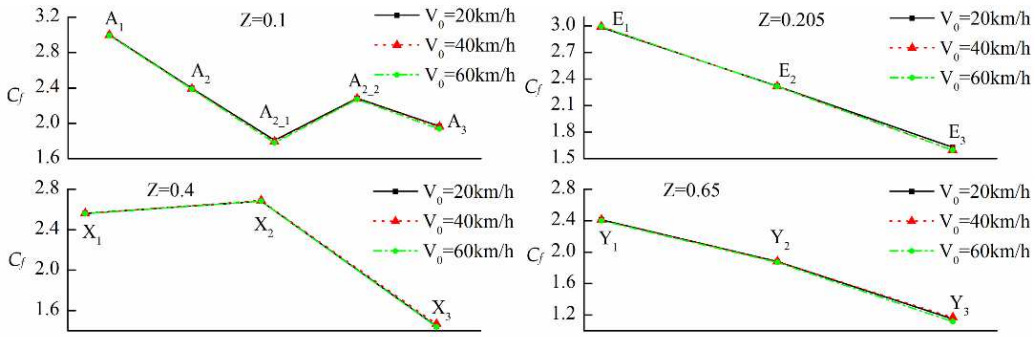

Figure 5 Multi-objective fitness value for each test point.

Figure 6 shows the dual-motor test platform that was developed to test the efficiency of the dual-motor system. Figure 7 presents the braking processes for distribution strategy points A_1 and A_3. The former is the optimal regenerative braking force distribution strategy proposed in this paper, while the latter is the traditional braking force distribution strategy without considering the effect of the non-work SMPMSM on braking performance. The average transfer

efficiency of the dual-motor system based on the optimal strategy proposed above was improved by 6.128% compared with the traditional one.

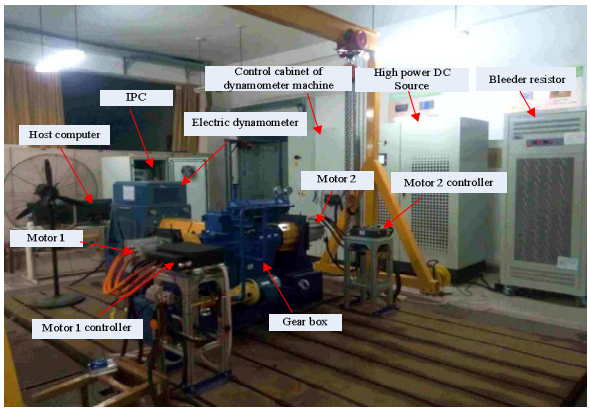

Figure 6 Dual-motor test platform.

5.3 Braking Energy Recovery Design Scheme Simulation

In order to verify the characteristics and rules of regenerative braking and energy feedback of different braking feedback schemes, the hardware-in-loop (HIL) platform as shown in Figure 8 was used to verify the proposed scheme. The HIL simulation platform was used to simulate the operating conditions of the dual motor electric vehicle to the maximum extent and shorten the period of strategy verification and development. Figure 9 presents the characteristics of the regenerative braking force and the braking energy recovery for various brake recovery strategies.

5.4 Discussions of the Simulation Results

Analysis of the experimental results shows that, under the influence of the braking stability factors, the energy feedback effect of Scheme 1 was the worst; the regenerative brake force distributed by the rear shaft motor was at its minimum. Compared with the first design, Scheme 2 performed better and Scheme 3 performed optimally. The main reason is that in Scheme 2, the regenerative braking force distributed by the front axle motor is significantly increased, while the rear axle regenerative braking system is not involved in the whole vehicle braking, so the energy feedback effect is moderate. Scheme 3 realizes dual motor four-wheel regenerative braking mode, which simultaneously ensures braking stability and energy recovery efficiency. Accordingly, Scheme 3 is the optimal braking recovery mode for the DMDEV. This conclusion validates the previous analysis.

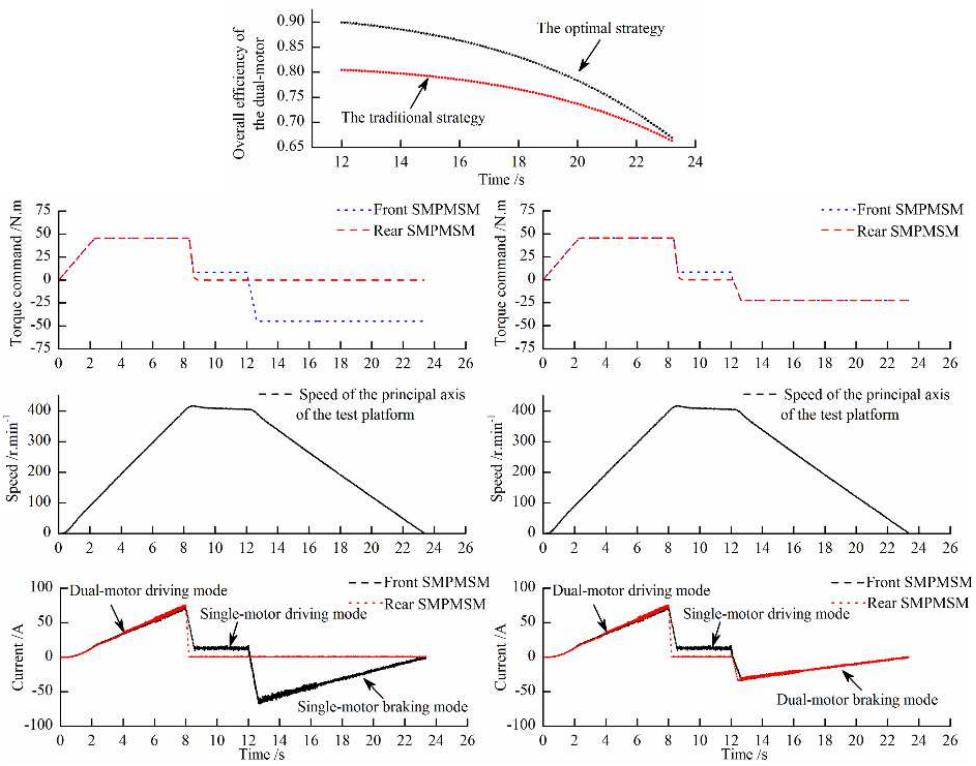

(a) The traditional braking force distribution A (b) The optimal braking force distribution A_1

Figure 7 Curves of the optimal and traditional braking force distribution for Case 4.

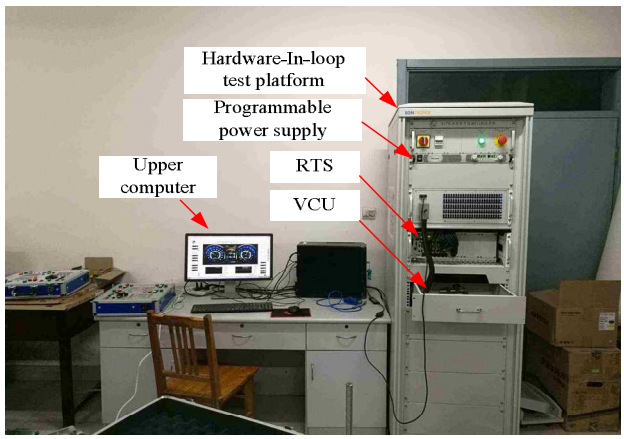

Figure 8 Hardware-in-loop simulation platform.

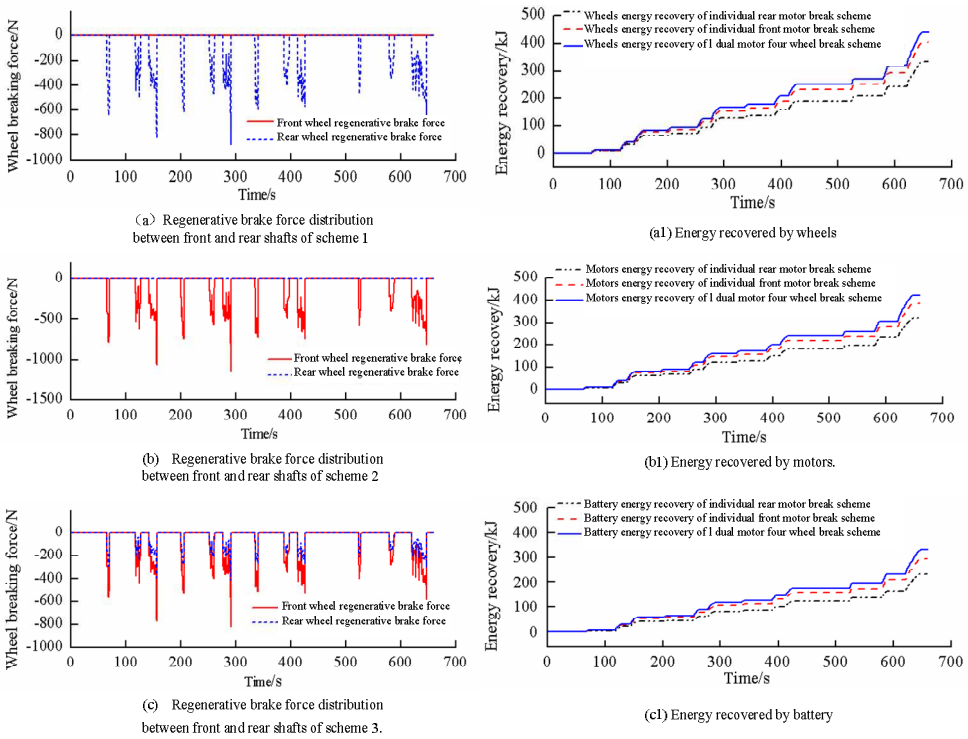

Figure 9 Effect of regenerative brake strategy on regenerative brake force distribution and energy recovery (based on a series parallel brake system).

Due to the influence of motor transmission energy loss and battery charging loss, the three regenerative braking feedback schemes above have the largest energy feedback at the wheels, followed by the motor energy feedback, while the battery energy feedback is minimal. Therefore, on the premise of meeting the braking stability constraint for DMDEV, the key factors to improve the braking efficiency of the whole vehicle are increasing the regenerative energy recovery at the wheels and enhancing the energy transfer efficiency of wheels to the battery. This study verified the qualitative and quantitative analysis results presented in our previous paper.

6 Conclusions and Future Scope

In this paper, braking force distribution strategies for a front-and-rear-SMPMSM-drive EV with a series braking system were investigated. Based on the loss mechanisms of SMPMSM, a new method was put forward to derive the optimal β aimed at improvement of energy transfer efficiency. Four evaluation

indexes (C_λ, C_β, $C\alpha_3$, C_f) were proposed to evaluate braking stability, energy transfer efficiency, energy recovery and braking force distribution strategy standard. The effects of the three key factors (λ, β and α_3) on braking stability and energy recovery were confirmed. More specifically, the obtained conclusions are as follows:

1. If the regenerative braking force distribution between two SMPMSMs is at low braking power conditions and the non-work motor loss is considered, the transfer efficiency of the dual-motor-brake-mode precedes the single-motor-brake-mode.
2. β is the key factor affecting energy recovery at low braking intensity ($C\alpha_3$ = 1). With the increase of braking intensity, the proportion of mechanical braking force increases and the effect of α_3 on energy recovery increases.
3. A reasonable braking force distribution strategy of a dual-SMPMSM-drive EV should consider breaking stability and braking energy recovery efficiency. Therefore, firstly, the braking force between the axles should adhere to the ideal curve of λ_I; secondly, a regenerative braking force is preferred; finally, the hydraulic braking system takes part in the cooperative brake only when the regenerative braking force is insufficient.
4. At high braking intensities ($Z > 0.7$), the braking recovery energy is very small. Only the hydraulic brake system is involved in braking to ensure safety.

In addition, deeper research is required to analyze the effect of C_β on energy transfer efficiency in a DMDEV with dual induction motors (IMs) or a configuration with IM and PMSM. Furthermore, the optimal braking force distribution strategy for dual-SMPMSM-drive EV with parallel cooperative braking system is still unknown.

Acknowledgements

This work was supported by the Natural Science Foundation of Shandong Province (grant no. ZR2018LF009) and the Scientific & Technological Support Plan of Shandong Province (grant no. 2015GGX105009).

References

[1] Santos, A., Mcguckin, N. & Nakamoto, H., *Summary of Travel Trends: 2009 National Household Travel Survey*, US Department of Transportation, Washington DC, 2011.

[2] Chan, C.C., Bouscayrol, A. & Chen, K., *Electric, Hybrid, and Fuel-Cell Vehicles: Architectures and Modelling*, IEEE Transactions on Vehicular Technology, **59**(2), pp. 589-598, 2010.

[3] Mutoh, N., Kato, T. & Murakami, K., *Front-and-Rear-Wheel-Independence-Drive-Type Electric Vehicle (FRID EV) Taking the Lead for Next Generation Eco-Vehicles*, SAE Paper, **39**, pp. 7206, 2010.

[4] TESLA, *Revolution of Automobile Engineering*, https://www.tesla.cn/models, accessed on April 17, 2015.

[5] Hong-Qiang, G., Hong-Wei, H. & Xiao-Kun, S., *Hierarchical Optimization Method for Regenerative Braking Stability of Hybrid Electric Vehicles,* Journal of Beijing Institute of Technology (English Edition), **23**, pp. 1-7, 2014.

[6] Binbin, S., Song, G., Zhe, W. & Junwei, L., *Parameters Design and Economy Study of an Electric Vehicle with Powertrain System in Front and Rear Axle*, International Journal of Engineering TRANSACTIONS A: Basics, **29**(4), pp. 454-463, 2016.

[7] Kang, J., Yoo, J. & Yi, K., *Driving Control Algorithm for Maneuverability, Lateral Stability, and Rollover Prevention of 4WD Electric Vehicles with Independently Driven Front and Rear Wheels*, IEEE Transactions on Vehicular Technology, **60**(7), pp. 2987-3001, 2011.

[8] Mutoh, N., Takahashi, Y. & Tomita, Y., *Failsafe Drive Performance of FRID Electric Vehicles with the Structure Driven by the Front and Rear Wheels Independently*, IEEE Transactions on Industrial Electronics, **55**(6), pp. 2306-2315, 2008.

[9] Wueng, C-C., Yang, Y-H. & Cheng, J-H. *An Improved Regenerative Braking Control Strategy and System for Dual Motor Electric Vehicle*, The 25th World Battery, Hybrid and Fuel Cell Electric Vehicle Symposium & Exhibition, Shenzhen, China, pp. 5-9, 2010.

[10] Antanaitis, D.B., *Effect of Regenerative Braking on Foundation Brake Performance*, SAE International Journal of Passenger Cars – Mechanical Systems, **3**(2), pp. 14-30, 2010.

[11] Li, L., Zhang, Y., Yang, C., Yang, B. & Martinez, C.M., *Model Predictive Control-based Efficient Energy Recovery Control Strategy for Regenerative Braking System of Hybrid Electric Bus*, Energy Conversion & Management, **111**, pp. 299-314, 2016.

[12] Afjei, E., Hashemipour, O., Saati, M. & Nezamabadi, M., *A New Hybrid Brushless Dc Motor/Generator without Permanent Magnet*, International Journal of Engineering Transactions B Applications, **20**(1), pp. 77-86, 2007.

[13] Guo, H., He, H. & Xiao, X., *A Predictive Distribution Model for Cooperative Braking System of an Electric Vehicle*, Mathematical Problems in Engineering, 2014 (3), pp. 1-11, 2014.

[14] Li, L., Li, X., Wang, X., *Transient Switching Control Strategy from Regenerative Braking to Anti-lock Braking with a Semi-brake-by-wire system,* Vehicle System Dynamics, **54**(2), pp. 257-283, 2016.

[15] Wang. F. & Zhuo, B., *Regenerative Braking Strategy for Hybrid Electric Vehicles Based on Regenerative Torque Optimization Control*, Proceedings of the Institution of Mechanical Engineers Part D: Journal of Automobile Engineering, **222**, pp. 499-513, 2008.

[16] Shi, Q., Zhang X. & Chen, F., *Multi-lookup Table based Regenerative Braking Strategy of Plug-in Hybrid Electric Vehicle*, Applied Mechanics and Materials, 44-47, pp. 1509-1513, 2011.

[17] Xu, W., Zheng, H. & Liu, Z., *The Regenerative Braking Control Strategy of Four-Wheel-Drive Electric Vehicle Based on Power Generation Efficiency of Motors*, SAE World Congress and Exhibition; Detroit, MI, United States, **2**, pp. 97364, 2013.

[18] Pennycott, A., De Novellis, L., Gruber, P. & Sorniotti, A., *Optimal Braking Force Allocation for a Four-wheel Drive Fully Electric Vehicle*, Proceedings of the Institution of Mechanical Engineers Part I: Journal of Systems and control Engineering, **288**(8), pp. 621-628, 2014.

[19] Shen, Q., Xu, F., Han, X., Tong, W. & Tang, R., *Investigation on the Variation of Iron Loss of Permanent Magnet Synchronous Traction Motor under Different Load Toque*, In: International Conference on Electrical Machines and Systems, pp. 1-5, 2011.

[20] Pennycott, A., De Novellis, L., Gruber, P., Sorniotti, A. & Goggia, T., *Enhancing the Energy Efficiency of Fully Electric Vehicles via the Minimization of Motor Power Losses*, In: IEEE International Conference on Systems, Man, and Cybernetics (SMC), pp. 4167-4172, 2013.

[21] Wang, R., Chen, Y., Feng, D., Huang, X. & Wang, J., *Development and Performance Characterization of an Electric Ground Vehicle with Independently Actuated In-wheel Motors*, Journal of Power Sources, **196**(8), pp. 3962-3971, 2011.

[22] Chen, Y. & Wang, J., *A Global Optimization Algorithm for Energy-Efficient Control Allocation of Over-Actuated Systems*, In: Proc. 2011 American Control Conference, San Francisco, CA, USA, pp. 5300-5305, 2011.

[23] Chen, Y. & Wang, J., *Energy-Efficient Control Allocation for Over-Actuated Systems with Electric Vehicle Applications*, In: Proc. 2010 ASME Dynamic Systems and Control Conf. (DSCC2010), Cambridge, Massachusetts, USA, pp. 37-44, 2010.

[24] Sangtarash, F., Esfahanian, V., Nehzati, H., Haddadi, S., Bavanpour, M.A. & Haghpanah, B., *Effect of Different Regenerative Braking Strategies on Braking Performance and Fuel Economy in a Hybrid Electric Bus Employing CRUISE Vehicle Simulation*, SAE paper: (01), p.1561, 2008.

[25] Ji, F. & Liu, L., *Study on Stability of Electro-Mechanical Hybrid Braking System in Electric Vehicles Based on ECE Regulation*, In: Proceedings-

International Conference on Computer Distributed Control and Intelligent Environmental Monitoring, CDCIEM, pp. 1358-1362, 2011.

[26] Qiu, B. & Chen, Q., *Evaluation Method of Regenerative Braking for Electric City Bus*, Journal of Mechanical Engineering, **48**(16), pp. 80-85, 2012.

[27] Simard, J. & Sarraillon, S., *Electric Vehicle Braking System*, U.S. Patent Application 10/459, 594, 2003.

[28] Urasaki, N., Senjyu, T. & Uezato, K., *An Accurate Modelling for Permanent Magnet Synchronous Motor Drives,* In: the 15th Annual IEEE Applied Power Electronics Conference and Exposition, New Orleans, Louisiana, USA, pp. 387-392, 2000.

[29] Seung-Ki, S., Zhang Y. & Liu, Z. *Motor Drive System Control*, Machinery Industry Press, Beijing, China, 2013.

[30] Lee, J., Nam, K., Choi, S. & Kwon, S. *Loss-Minimizing Control of PMSM with the Use of Polynomial Approximations*, IEEE Transactions on power electronics, **24**(4), pp. 1071-1082, 2009.

[31] Gieras, J.F. & Wing, M., *Permanent Magnet Motor Technology*, *Design Applications*, 2nd ed., Marcel Dekker, Inc., pp. 1181-1187, 2002.

[32] Economic Commission for Europe, *Uniform Provisions Concerning the Approval of Vehicles of Categories M, N and O with Regard to Braking,* Addendum 12, Regulation No.13, 2008.